Seismic Tomography With Irregular Meshes

Malcolm Sambridge and Nick Rawlinson

Centre for Advanced Data Inference, Research School of Earth Sciences, Australian National University, Canberra

Short title: TOMOGRAPHY WITH IRREGULAR MESHES

Article published as

Seismic Tomography with Irregular Meshes
Sambridge, M. and Rawlinson, N., 2005. *Seismic Earth: Array Analysis of Broadband Seismograms*, *Geophysical Monograph Series 157*, Eds. A. Lavender and G. Nolet, , 49-65, 10.1029/156GM04.

Abstract. The current state of seismic tomography using irregular parameterizations is described. A review is given of previous work in the area covering local, regional and global seismic applications. The potential advantage of an irregular parameterization over a regular (uniform) one is that, by introducing higher resolution grids in particular parts of the model, one can maximize the information extracted from the data. Although irregular parameterizations have only recently been used in 3-D mantle tomography, their origins can be traced back more than twenty years.

The use of irregular meshes in two and three dimensional tomographic imaging creates a number of 'implementation' issues, not seen with uniform grids. An outline of algorithms for solving all of these bookkeeping problems arising in cubic, tetrahedral or polygonal meshes is included, and references given to more detailed descriptions. Some recent implementations of tomography are discussed where the parameterization is refined during the course of the inversion process. Two examples of adaptive tomography in non-seismic problems suggest that the gradual refinement of the parameterization may be an effective way to regularize the inverse problem.

The intention here is to point out the potential advantages and pitfalls of using an irregular parameterization in tomography. At present experience with seismic problems is rather limited (especially in 3-D) and an optimal approach is yet to emerge.

1. INTRODUCTION

Tomographic imaging of mantle structure has been a favored tool of seismologists for more than twenty years, and has resulted in numerous 3-D models of the Earth's interior. Summaries can be found in *Romanowicz* [1991], *Iyer and Hirahara* [1993], *Nolet et al.* [1994], *Ritzwoller and Lavely* [1995], *Dziewonski* [1995], and *Masters and Shearer* [1995]. In recent years both the abundance and quality of body wave and surface wave data have increased dramatically. At the same time the consistency between the 3-D models has also improved (see *Grand et al.* [1997] for a discussion). However, it has long been recognized that the limited geographical distribution of seismic sources and receivers on the Earth's surface leads to (often) highly irregular sampling of the mantle (especially for body wave studies). This in turn places fundamental restrictions on the amount of information on lateral heterogeneity that can be extracted. In particular one would expect that large variations in ray path density lead to large variations in the resolving power of the data.

Traditionally tomographic studies have largely ignored the (lateral) spatial variability in the datas' resolving power and opted to build models in terms of uniform local or globally supported basis functions, e.g. cubic cells or spherical harmonics (see Figure 1). The type of parameterization combined with spatial smoothing and damping procedures, effectively limit both the size and length scale of lateral variations in the resulting Earth models. More recently seismologists have focused on ways of maximizing the extraction of structural information from data. To this end one

approach that is receiving increasing attention is to perform tomographic inversions with parameterizations which are themselves laterally varying, and are in some sense tuned to the resolving power of the data.

The use of an irregular parameterization in tomography is complicated by a number of factors, not least of which is the need for some sophisticated computational algorithms for building, storing and searching through an irregular 2-D or 3-D mesh, and then representing Earth properties on such a mesh. A range of approaches have been proposed and applied to various tomographic problems. The purpose of this article is to summarize those studies and comment on the relative merits of the approaches adopted. We describe the basic geometric issues that must be considered when building irregular parameterizations, and outline some efficient techniques for dealing with them. We also describe some new ideas taken from other non-seismic tomographic problems, where adaptive parameterizations have also been a subject of recent interest. We finish with some examples of tomographic applications using adaptive parameterizations over local, regional and global distances.

2. A BRIEF REVIEW OF TOMOGRAPHY IN IRREGULAR MESHES

2.1. Why use an Irregular Parameterization ?

The primary motive for adopting an irregular parameterization is to maximize the amount of information extracted from the data. But how do we know that uniform

parameterizations do not already extract all of the available (coherent) information in the data ? It seems reasonable to suspect this to be the case because the minimum scale length allowed in uniform parameterizations (e.g. block size or number of harmonics) is often chosen as a compromise between data constraint and computational convenience. In 3-D global tomography with blocks one might well believe that the arrival time data could resolve structure smaller than the block size in regions of highest data density, however merely halving the block size would increase the number of unknowns by a factor of eight. A similar nonlinear dependence of inversion variables with spatial scale length occurs in spherical harmonic representations.

Direct evidence is also provided by examining how well uniformly parameterized tomographic models fit global P-wave travel time data. Plate 1 shows the data fit of 1-D and 3-D global P-wave models for arrival times observed at station MAT in Japan (42° north of the center of the figure). Residuals are shaded according to their size and plotted as a function of source position in an $\sim 20^\circ \times 20^\circ$ region centered on Indonesia. Plate 1a shows the observed residuals (with respect to the 1-D model *ak135* [*Kennett et al.*, 1995]. Plates 1b and 1c show the predicted residuals for the whole mantle spherical harmonic model MK12/WM13 of *Su and Dziewonski* [1995] and the uniform block model of *Gorbatov et al.* [2001], respectively. (Note here that a 'predicted residual' is the travel time calculated through a 3-D model minus the *ak135* time.)

The observed residual pattern in Plate 1a shows correlation over multiple distance scales indicating the influence of Earth structure somewhere between source and receiver. The southern most events lying at the top of the subduction zone are fast

while the deeper events (slightly further north) are slow, which clearly corresponds to ray paths traveling through the slab to the station (MAT) which lies NNE of the region. Elsewhere, and especially in the central northern region, correlated residuals appear within similar depth ranges suggesting lateral heterogeneity. The long wavelength spherical harmonic model (Plate 1b) shows laterally correlated residuals which poorly fit the observed pattern over these distance ranges. This is not entirely surprising since the smallest wavelengths allowed in the 3-D model correspond to approximately 1500 km, which is much longer than the scale length of the observed signal. The predictions from the block model (Plate 1c) are better but do not account for all of the variations seen in Plate 1a. In this case the uniform block size corresponds to approximately 200 km. Overall these figures show that there is significant unmodelled (regional) signal in the observed residuals which is not represented in uniformly parameterized global models.

Plates 1d, 1e, and 1f show the auto-correlation functions of the residuals for the three Earth models. Note that we have plotted the auto-correlation function of the observed minus the predicted arrival time in each case as a function of source separation. If a velocity model accounted for all of the spatially correlated signal in the data, and left only uncorrelated random noise we would expect to see no variations in the auto-correlation with source separation. This is an alternative way, to the usual variance reduction, of measuring how well a velocity model fits data. Plate 1d shows the effects of lateral heterogeneity seen in 1a. Plate 1e shows that the spherical harmonic model results in virtually no reduction in the auto-correlation over the 1-D model, while the block model, being more sensitive, is able to do better, although structure is still

apparent.

By examining both the spatial variation in residual patterns and the auto-correlation plots one clearly sees that global models do not fit regional variations particularly well. If one were to choose a uniform block model with length scales equivalent to the smallest distance lengths seen in Plate 1a, then the increased number of unknowns would make the tomographic system computationally prohibitive. Even if solutions were obtained, they would be unlikely to be optimal in the sense of extracting maximum information from the data. Currently the only way of capturing the range of length scales seen in the data is to vary the density of the mesh spatially.

2.2. Previous Studies

The use of variable 2-D and 3-D meshes in tomography goes back quite some time. *Chou and Booker* [1979] and *Tarantola and Nercessian* [1984] were well aware of the limitations of a fixed uniform grid and proposed 'block-less' parameterizations for seismic tomography. These allowed the local smoothing scale lengths to vary spatially and were, in principle, very similar to subsequent variable mesh schemes. Later *Williamson* [1990] and *Sambridge* [1990] used 2-D and 3-D grids which gradually decreased their cell size as iterations proceeded. In the context of regional arrival time tomography *Fukao et al.* [1992] used non-uniform sized rectangular 3-D blocks to account for uneven ray path sampling. *Abers and Roecker* [1991] introduced a scheme where fine scale regular 3-D blocks are joined to form larger irregular cells, and applied the technique to image P-wave velocity structure beneath Papua New Guinea.

In the inversion of 2-D crustal refraction data *Zelt and Smith* [1992] adjusted the trade-off between data fit and resolution by using a layered variable block representation built around variably spaced nodes. *Sambridge et al.* [1995] and *Sambridge and Gudmundsson* [1998] were the first to propose the use of Delaunay tetrahedra and Voronoi polyhedra for tomographic problems. These are completely unstructured meshes, i.e. not based on a cubic or other regular grid [*Voronoi* 1908; *Okabe et al.,* 1992] (see also Figure 6). Delaunay tetrahedra and Voronoi polyhedra were used by *Gudmundsson and Sambridge* [1998] to develop a Regionalized Upper Mantle (RUM) reference Earth model.

Michelini [1995] introduced an adaptive grid method for 2-D cross-hole tomography using cubic B-splines; both the velocity model and the positions of the nodes were updated at each iteration. *Vesnaver* [1996] looked at a 2-D reflection problem and deformed the (pixel) cell boundaries to eliminate rank deficiency in the tomographic system of equations. Adopting a similar philosophy *Curtis and Snieder* [1997] considered a 2-D cross-borehole problem and represented structure using a Delaunay triangulation built around a set of nodes. They used a genetic algorithm to find the position of the nodes which minimized the condition number of the resulting tomographic systems of equations. The object here was also to maximize model resolution in the 2-D velocity model.

In a surface wave study *Wang et al.* [1998] used a mesh built from spherical triangles subdivided in regions of higher data density (similar to that shown in Figure 2b). In mantle tomography *van der Hilst et al.* [1997] and *Widiyantoro and van der*

Hilst [1997] increased the resolution of their mesh in target regions by embedding high resolution regular meshes within an otherwise globally uniform grid. A similar approach was adopted by *Zhou* [1996]. *Bijwaard and Spakman* [2000], *Bijwaard et al.* [1998] and *Spakman and Bijwaard* [2001] performed global P-wave tomography using a variant of the *Abers and Roecker* [1991] approach where the variable 3-D grid is chosen to match variations in ray path density. This is probably the most successful example of 'static' grid whole Earth tomography to date.

Vesnaver et al. [2000] and *Böhm et al.* [2000] developed an adaptive scheme for 3-D reflection tomography using Delaunay triangles and Voronoi polyhedra to track the gradients in velocity and ray path density. *Chiao and Kuo* [2001] proposed a multi-scale parameterization based on 2-D spherical wavelets, and used it to estimate shear wave heterogeneity in the D'' layer. Very recently *Sambridge and Faletič* [2003] performed whole Earth P-wave tomography in an adaptive grid (i.e. one that updates during the inversion) using Delaunay tetrahedra (an example of their approach is discussed in section 4.3). Utilizing the flexibility of tomographic schemes built around Delaunay and Voronoi meshes is also the subject of ongoing work [e.g. *Montelli et al.* 2001].

3. COMPUTATIONAL TOOLS AND TECHNIQUES

3.1. Basic Building Blocks

The impediments to using an irregular parameterization in seismic tomography include the computational problems that arise from implementing any particular scheme,

and the subsequent difficulty in interpreting results. In this section we consider the first issue. (In section 4 we offer some comments on the interpretation question.)

The common element in all tomographic studies is to represent a 2-D or 3-D seismic velocity, or slowness field, $m(\mathbf{x})$ as a linear sum of basis functions

$$m(\mathbf{x}) = \sum_{i=1}^{N} \lambda_i \phi_i(\mathbf{x}) \tag{1}$$

where λ_i are the unknowns solved for in the inversion. Many choices of basis function $\phi(\mathbf{x})$ are possible. Here we only consider basis functions with 'local support', which means that they are only non-zero within a limited sub-region of the entire model. Simple examples would be constant slowness cells with rectangular (cubic in 3-D) or triangular (tetrahedral in 3-D) geometries. The ease with which uniform rectangular meshes may be implemented (see below) has led to it being by far the most commonly used in seismic studies [see *Iyer and Hirahara* 1993, for many examples].

A well known drawback of rectangular meshes, in mantle tomography, is the distortion effect near the poles. Equi-spaced longitude cells lead to gradual distortion as a function of latitude and high concentrations near the poles. This problem is avoided by using spherical triangular meshes [*Constable et al.* 1993; *Wang and Dahlen* 1995]. Figure 7 shows an example of two uniform spherical triangle meshes on a sphere.

An alternative to uniform cell parameterizations is to allow gradients across each cell by defining the unknowns as the slowness value at the vertices of each element (see Figure 2). In this case linear interpolation is possible within triangular and tetrahedral elements [see *Williamson* 1990], while bi-linear (tri-linear) interpolation is convenient in

rectangular (cubic) elements [see *Thurber* 1983; *Eberhart-Phillips* 1986]. Even higher orders of smoothness can be imposed using splines defined at the nodes of each cell. Various types of splines have been popular in 2-D and 3-D studies [*Thomson and Gubbins* 1982; *Lutter and Nowack* 1990; *Sambridge* 1990; *Neele et al.* 1993; *VanDecar et al.* 1995; *Rawlinson et al.,* 2001a]. In each case the particular interpolation used corresponds to a set of basis functions $\phi(\mathbf{x})$ and the summation in (1) is used to construct the slowness field.

Both rectangular and triangular elements lend themselves to an irregular parameterization. Figure 2 shows examples built from 'self-similar sub-divisions' of each element. In each case new elements are formed by simply dividing the edge of a larger element in two. For the rectangular and triangular mesh a sub-division produces four new similar shaped cells with area exactly a quarter of the original. In the 3-D case a sub-division of the cube and the tetrahedron results in eight new elements, but only in the cubic case are they all identical.

Clearly the smaller elements represent a local refinement of the parameterization, and this is most easily implemented if constant slowness basis functions are used in each element. (The surface wave study of *Wang et al.* [1998], see also *Wang and Dahlen* [1995], is a rare example of a higher-order spline basis function combined with an irregular 2-D spherical mesh.) In practice a drawback with the sub-division approach is that a large number of new unknowns are introduced with each sub-division, i.e. for cases in Figures 2a-2d we have 4, 4, 8 and 8 respectively. This can quickly become computationally prohibitive if many cells are subdivided at each iteration.

All examples in Figure 2 are what we might call 'top down' irregular parameterizations, i.e. where larger cells are sub-divided into smaller cells. An alternative is a 'bottom up' style, where small elements are joined together to produce new cells of arbitrary shape. (The three cases in Figure 5b serve as examples where the different shaded regions are all built from smaller square cells.) The bottom up approach has already been used to considerable effect in the 3-D seismic tomography studies of *Fukao et al.* [1992], *Abers and Roecker* [1991], *Bijwaard et al.* [1998] and *Spakman and Bijwaard* [2001]. In these cases, however, the parameterizations are 'static', in that the mesh is not updated during the inversion, but rather chosen to reflect variations in ray path density (in a reference model) and then held fixed. This is reasonable because, even in a nonlinear inversion with 3-D ray tracing, the ray path densities may not vary sufficiently between iterations to justify updating the mesh.

In contrast to the bottom up approach, the top down technique has no lower bound on the size of the element, and is perhaps more suited to an adaptive parameterization, i.e. one in which the mesh is updated (according to some criteria) and the tomographic system of equations are re-solved in each new parameterization. An example is given by *Faletič* [1997] and *Sambridge and Faletič* [2003] (see also section 4.3).

3.2. Bookkeeping Problems in Unstructured Meshes

Ultimately the irregular parameterization style must be chosen to suit the details of the particular application. However, the ease with which each type can be implemented varies considerably due to the 'bookkeeping problems' that arise in the formulation of

the tomographic system of equations

$$\mathbf{A}\delta\mathbf{x} = \delta\mathbf{d}. \tag{2}$$

Here $\delta\mathbf{x}$ is the vector of unknowns (i.e. perturbations of the coefficients λ_i from some reference Earth model), and $\delta\mathbf{d}$ is the data vector (usually residuals of observed and predicted reference model travel times).

For any parameterization (uniform or irregular) the entries in coefficient matrix $\mathbf{A}$ are determined by integration of the basis functions, $\phi_i(\mathbf{x}), (i = 1, \ldots, N)$ along the rays in the reference Earth model. This process will be familiar to many readers, and is illustrated in Figure 3. Specifically $A_{i,j}$ is equal to the integral of the ith basis function, $\phi_i(\mathbf{x})$, along the jth reference ray, R_j,

$$A_{i,j} = \int_{R_j} \phi_i(\mathbf{x}) ds. \tag{3}$$

For constant slowness cells of any shape one arrives at the usual result [see e.g. *Shearer* 1999] that $A_{i,j}$ is equal to the length of the jth ray in the ith cell.

In the general case the integration along each ray may be performed numerically using, for example, a simple Runge-Kutta technique [see e.g. *Press et al.* 1992]. Of course in the constant slowness case we need only count up the ray segments falling into each cell, regardless of its shape. In all cases then, the central bookkeeping problem to be solved is to find in which 2-D or 3-D cell any given point along the ray falls. If iterative non-linear tomography is used and ray paths are re-traced between each model update, then similar processes are required in order to propagate the paths through the mesh. [Note in special cases where the length of the reference ray has an analytical

expression the central problem can become one of finding the intersection of the ray segments with the cell boundaries.]

In uniform rectangular meshes this is a trivial task, which can be solved by simply using the co-ordinates of the point and the definition of the regular grid. This is perhaps the reason why regular fixed grids have remained popular in tomography for so long. In all irregular meshes (2-D or 3-D) the solution requires both a data structure to store the mesh, and an algorithm to search that data structure to locate the cell containing any particular point. For sub-divided rectangular based elements (Figure 3a and 3c) quad-trees (in 2-D) and octrees (in 3-D) are ideal for the purpose and allow a very efficient point location algorithm [*Bentley* 1975, *Samet* 1995].

In all sub-divided meshes like that shown in Figure 2, the location problem is essentially one of repeatedly finding the cell surrounding the point in each level of the mesh. For example in the case of Figure 2c, a point in the smallest gray cube could be found by first determining in which of the eight half-sided cubes it lies, and then in which of the eight quarter-sided cubes (i.e. inside the previously located half-sided cube). This is how quad-trees and octrees work, but the same general idea can be used for sub-divided meshes of more complex shape, e.g. triangles, tetrahedra or triangular prisms.

For arbitrarily shaped 2-D and 3-D polygons, 'point location' is a much studied problem [see e.g. *Okabe et al.* 1992], and many algorithms exist. A particularly simple one which allows location in any 2-D or 3-D convex polyhedra may be stated as follows. Suppose we have a 2-D parameterization consisting of N arbitrarily convex polygons,

and for each we have a point $\mathbf{p}_i$ $(i = 1, \ldots, N)$, inside of the polygon (Figure 6 serves as an example). Suppose also that we have a table $n(i, j)$ $(j = 1, \ldots, E_i; i = 1, \ldots, N)$ which tells us the index of the jth neighbouring polygon, i.e. the one which shares edge j with polygon i. Here E_i is the number of edges of polygon i (note we write $n(i, j) = 0$ if the j edge is on the boundary of the parameterization). We can locate the polygon containing any given point, $\mathbf{x}$, using the following procedure:

1. Choose any starting polygon k;
2. For $j = 1, \ldots, E_k$; (loop over edges of polygon k)
   - Is $\mathbf{x}$ on the same side of edge j as $\mathbf{p}_k$?
     - → If no:
       - ▷ If $n(i, j) = 0$, **stop**: $\mathbf{x}$ must be outside of mesh.
       - ▷ Set $k = n(i, j)$;
       - ▷ go to (2); (repeat procedure for new polygon)
     - → If yes: continue (consider next edge of polygon k)
3. End loop
4. **stop**: Point $\mathbf{x}$ must be in polygon k.

The geometric problem in step 2 can be solved with some simple vector algebra. Indeed one can often use one of the vertices of the polygon in place of a separate point $\mathbf{p}_k$. See *Sambridge et al.* [1995] and *Sambridge and Gudmundsson* [1997] for details of both 2-D and 3-D cases. In most cases the neighbouring table $n(i, j)$ can be built at the same time as the mesh. Details of algorithms can be found in *Sambridge et al.* [1995].

The convexity of the cell boundary allows the algorithm to be immediately carried over to the 3-D case, with faces replacing edges and so on. Usually it is quite efficient because only a small number of polygons need to be tested. Figure 4 shows an example

of its application to a triangular network, with starting guess far from the solution triangle. Note that a near direct walk is made between the starting guess and the solution. We recall that in the application to tomography an evaluation of the integral (3) requires stepping down a reference ray (Figure 3), and so the search for each new point can use the polygon for the previous point as a starting guess, which can make the overall procedure very efficient.

This technique may also be applied to non-convex polyhedra if they can be broken down into simpler convex regions, e.g. as in a parameterization built in a 'bottom up' fashion. For example in Figure 5b (far right panel) point location in the non-convex shaded region is accomplished by simply locating the individual square containing the point, each of which is associated with one of the two larger regions. More sophisticated variants are required for arbitrary non-convex polyhedra, but to date these have not been used in tomographic problems.

3.3. Adaptive Parameterization in Seismic Tomography

Having outlined mechanisms for building irregular 2-D and 3-D parameterizations for tomographic problems, and calculating coefficients of the corresponding linear system, we now turn to the question of how to iteratively adapt the parameterization during the inversion process. This is a relatively new area as far as mantle tomography is concerned. As mentioned above nearly all 3-D tomographic studies which have used an irregular mesh are 'static' in that the mesh is fixed beforehand, usually chosen to mimic variations in ray density. With an adaptive parameterization the mesh itself becomes

part of the inversion process, and some criteria must be introduced to drive changes in an iterate fashion. Since experience with adaptive seismic tomography is rather limited, there appears, as yet, to be no consensus on how best to refine a parameterization. In section 4.3 we show some examples from the work of *Faletič* [1997] and *Sambridge and Faletič* [2003] who used slowness gradients imaged in a tomographic model to drive the subsequent refinement of a 3-D parameterization.

Recently, some schemes for adaptive parameterization have been proposed for several non-seismic tomography problems. Two notable works are by *Grimstad et al.* [2002] and *Ben Ameur et al.* [2002]. In both cases a sequence of 2-D tomographic problems are solved in grids with an increasing number of unknowns.

The procedure of *Grimstad et al.* [2002] was applied to permeability estimation problems arising in reservoir engineering, and is illustrated in Figure 5a. It is an adaptive multi-scale approach similar to that described above; however, for each proposed refinement (from a restricted class of possibilities) an estimate is made of the likely improvement in data fit that will result, together with a measure of the uncertainty in that improvement. From this it is possible to decide which of the proposed new parameterizations is likely to give the highest reduction in data misfit for the least number of extra unknowns. Figure 5a shows a very simple case over two successive stages. Note here that for each new proposed 'candidate parameterization' the corresponding system of linear equations is not actually solved. The predicted changes in data fit can be determined in advance using the derivatives of the data misfit with respect to the new parameters, i.e. the coefficient matrix $A_{i,j}$ in (2). If, as in

Figure 5a, the parameterization is built on top of an underlying uniform grid (i.e. the bottom up approach) then all required derivatives can be found by summing up those corresponding to the underlying cells.

The adaptive parameterization technique developed by *Ben Ameur et al.* [2002], has some similarities to this approach and was applied to the estimation of hydraulic transmissivities. Again a series of new candidate parameterizations are produced at each stage, but in this case they are generated by slicing the current model with a restricted family of cuts (see Figure 5b). Each new cut may produce multiple new 'zonations', which become unknowns in the next parameterization. 'Refinement' and 'coarsening' indicators are calculated to decided which new parameters to allow and which to merge with existing variables. As in the multi-scale approach, derivatives of data misfit with respect to proposed parameterizations are used to predict which candidate parameterization should be retained and which rejected.

The schemes of *Grimstad et al.* [2002] and *Ben Ameur et al.* [2002] involve gradual refinement of a parameterization with relatively few extra unknowns added at each stage. In this sense they use the adaptive refinement as a way of regularizing the tomographic problem. The intention at each refinement is to introduce the least number of new parameters and obtain the greatest improvement in data fit. Perhaps the most interesting aspect is their use of local derivative information to 'predict' the performance of any proposed new parameterization. At present, this idea does not appear to have been used in seismic tomography. For 'bottom up' parameterizations, built on an underlying fixed grid (see Figure 5b), the derivatives would only need to be calculated

once and then summed together to produce the necessary prediction indicators. In principle these techniques could be applied to 2-D seismic imaging problems, e.g. cross-borehole tomography. It is not clear whether they would be practical in 3-D seismic tomography, because the number of potential parameterizations would grow rapidly with the size of the mesh. Nevertheless this might be an interesting area for further study.

4. SEISMIC APPLICATIONS OF IRREGULAR MESHES

Here we briefly describe three examples of tomographic problems where irregular meshes have been used. The three examples use different types of seismic data and span the local, regional and global distance scales. They also illustrate the different ways irregular meshing tools can be used: in the first as a way of representing an interface irregularly sampled by body waves; in the second as a measure of lateral resolution in surface wave data; and the third to represent a fully 3-D mantle model in adaptive tomography.

4.1. Crustal Seismics: Imaging Interfaces

Seismic imaging at crustal scales commonly involves the use of controlled sources such as explosives, air-guns and vibroseis. A significant advantage of controlled sources compared to earthquakes is that one is able to impose greater constraints on the nature of the data coverage. However, for a variety of reasons (logistical, geographical, financial, cultural etc.), an optimal coverage of sources and receivers is often hard to achieve, and

heterogeneous path coverage remains an issue with many of these datasets, especially those created using 3-D arrays.

Rawlinson and Sambridge [2003] examine the use of irregular meshes in the imaging of interface structure with 3-D wide-angle seismic data. Wide-angle data is recorded by receivers at significant offsets to surface sources, and typical seismograms exhibit both refracted and reflected phases. The presence of reflected arrivals allows the geometry of sub-surface interfaces to be imaged. The tomographic method used by *Rawlinson and Sambridge* [2003] was first presented by *Rawlinson et al.* [2001a], and uses a shooting method of ray tracing to determine source-receiver paths and travel times, and a subspace inversion method to solve the inverse problem. Structure is represented by a set of sub horizontal layers separated by smoothly varying interfaces. Within a layer, velocity varies linearly with depth, and each interface is described by a mosaic of cubic B-spline surface patches in parametric form. A grid of control vertices describe the shape of the surface patches. Surfaces described in this way may be multivalued, are C_2 continuous, and importantly may be composed of surface patches of different sizes and shapes. This latter property stems from being able to arbitrarily locate control vertices, although it should be noted that a rectangular association still exists between control vertices on the grid.

Of the suite of examples presented by *Rawlinson and Sambridge* [2003], there is one that investigates the use of irregular interface meshes with observed data; we focus on this example here. The wide-angle dataset used was recorded in Tasmania, SE Australia, in 1995 by Geoscience Australia (formerly the Australian Geological Survey

Organisation) and consists of recordings from 44 portable analogue and permanent digital stations distributed throughout Tasmania. Approximately 36,000 air gun shots were fired from the research vessel *Rig Seismic* as it circumnavigated Tasmania during the course of the experiment, and the travel time of this energy to the receiver array was used to constrain the structure of the Tasmanian crust.

In an earlier article, *Rawlinson et al.* [2001b] inverted 2148 P_mP and 442 P_n travel times from this dataset for the structure of the Moho surface using the scheme outlined above. However, they used a regular parameterization which described the Moho by 600 nodes spaced 20 km apart in orthogonal directions. The uneven distribution of data (see Plate 2a) which characterizes this component of the dataset clearly lends itself to an irregular parameterization because there is a distinct lack of paths in central and NE Tasmania. *Rawlinson and Sambridge* [2003] perform the same inversion but instead describe the Moho with an irregular grid of only 240 nodes, which is less than half the number used in the regular inversion. The nodes were positioned according to ray path coverage through the initial model and were not horizontally repositioned during the course of the inversion (i.e. a static irregular parameterization was adopted) The initial RMS data misfit of 371 ms (corresponding to a horizontal Moho) is reduced to 191 ms after four iterations. Despite the much smaller number of nodes, this misfit is only slightly greater than the 176 ms final misfit achieved by the regular grid inversion.

Plate 2 shows the results of the irregular grid inversion and the regular grid inversion. A comparison of Plate 2c and 2d shows that the resolution (calculated from linear theory) of the irregular parameter solution is generally superior to that of

the regular solution. In fact, towards the center of Tasmania, resolution has become non-zero. This indicates that model structure in this region is now influenced by the data to some extent. In comparing Plate 2e and 2f, we see that crust is thicker near central Tasmania in the irregular model compared to the regular model - this is consistent with the increased surface elevation in this region. However, the low resolution values associated with central Tasmania (Plate 2c) mean that we should treat this result with caution.

Another noticeable difference between Plate 2e and 2f is that the irregular solution reveals a broad scale shallowing in the NE of Tasmania that is both less distinct and less well resolved in the regular solution. The location of this feature coincides with the location of the Northeast Tasmania Element, a tectonic element with a distinct surface geology that was juxtaposed with western Tasmania during the Mid-Devonian Tabberabberan Orogeny. Evidence from coincident reflection data and a previous refraction survey also indicates a thinning of the crust beneath the Northeast Tasmania Element. In summary, the crustal scale example presented here endorses the use of an irregular parameterization in the presence of a heterogeneous data distribution.

4.2. Surface Waves: Resolution Measures

At the surface of the Earth, the distribution of surface wave paths is controlled by the positions of available events and stations and is almost always uneven. As a result surface wave studies can often result in very heterogeneous data sets, as for example when studying a region that covers both oceanic and continental areas. In the oceanic

zones few seismic stations are available so paths are sparse, but in continental areas the number of measurements and the path density continuously increases with the deployment of portable seismometers. Figure 6a shows an example of surface wave ray paths across the Australian continent, (derived from broadband deployments) and the Indian ocean (largely from permanent receivers).

This type of data set presents challenges because of the laterally variable resolving power of the data, which is controlled both by the physics of the problem (e.g. the wavelength of the seismic waves) and the density of seismic rays sampling the structure. *Debayle and Sambridge* [2004] propose the use of an irregular parameterization for this type of data set.

Starting from observed ray paths, a set of Voronoi cells on the Earth's surface can be defined about the points where two or more ray paths cross. Such Voronoi cells are 'nearest neighbour' regions around the crossing points. An example is shown in Figure 6b. Note that the size and shape of the cells is adapted to the path density, with large cells in regions poorly sampled by the data and smaller cells where the data allow better resolution. *Debayle and Sambridge* [2004] produced their 'resolvable Voronoi diagram' by first building nearest neighbour regions about all ray crossing points (which amounts to many thousands) and then gradually deleting the cross over point cells that did not satisfy a 'quality criterion'. This is a measure based on ray path density and angular distribution which ensures resolution of anisotropic structure in each cell. By iteratively removing poorly resolved cells and re-calculating the Voronoi diagram of the remaining points, one eventually arrives at a set of cells where all criteria are met by all cells. Note

that in the Tasman sea the ray density is high, but many paths have similar east-west orientations and hence result in poorer resolution, which is reflected by larger elongated Voronoi cells in Figure 6b.

The final Voronoi diagram reflects the information contained in the data set and may be used as either a measure of resolution available in different parts of the Earth, or as the basis of a new parameterization in surface wave tomography.

4.3. Global Travel Times: Adaptive Whole Earth Tomography

Sambridge and Faletič [2003] performed a tomography study of the mantle using a mesh composed of Delaunay tetrahedra. [This followed on from earlier work by *Faletič* 1997.] Their study was based on the data set of *Widiyantoro and van der Hilst* [1997], consisting of approximately 550,000 summary rays of P and pwP phases derived from 6 million arrival times from 77,000 events. They were able to perform 3-D whole mantle tomography with an adaptive tetrahedral parameterization.

Starting from a mesh of Delaunay tetrahedra built around 18 layers of uniformly distributed nodes generated using the approach of *Wang and Dahlen* [1995] (see Figure 7), new nodes were added at the edges of tetrahedra where the local velocity gradient was highest (see Figure 2d). The intention was to refine the parameterization in regions where the Earth structure was changing the most from the reference model. After adding new nodes a completely new tetrahedral mesh was constructed, and the process repeated. Four mesh updates were used, and for each update a tomographic system was solved using a conjugate gradient algorithm.

This is a slight departure from the refinement schemes discussed in section 3.1, because a complete tetrahedral mesh is obtained at each stage, rather than one with tetrahedra embedded within each other, as in Figure 2d. This has the advantage that the mesh construction can be performed with standard algorithms (e.g. the *quickhull* algorithm of *Barber et al.* [1993]) for which standard software exists. The tomographic system of equations can also be built using the procedures described in section 3.2. The disadvantage is that the tetrahedra can become quite distorted in the 3-D volume, even though, with a Delaunay tetrahedral mesh, one gets the least distortion possible for a given set of nodes. A second disadvantage is that the number of tetrahedra and hence unknowns to be solved for increases significantly as the mesh is refined.

Figure 8 shows a slice at 1300 km depth through the tetrahedral mesh produced in the first of four refinements. One notices that local refinement has occurred in all regions where major features are seen in other tomographic images at this depth, i.e. the Tethys ocean region, central Americas (corresponding to the Farallon plate), southern Africa (great African plume), Mediterranean and Tonga Kermadec subduction zone. An enlargement of the final irregular mesh (i.e. after four refinements) is shown in Figure 9. This is a slice at about 500 km depth. Considerable detail has been built into the mesh in the south western part of the Pacific plate where subduction results in lateral heterogeneity.

The idea of refining the parameterization in regions where model perturbations are highest is rather appealing because we would naturally want more detail where there are more lateral variations to image. However there is no guarantee that the

data can necessarily resolve such structures. Indeed if appropriate (explicit) damping and smoothing of the tomographic models is not sufficient, then conceivably this 'follow the model perturbations' approach may even enhance instabilities caused by local under-parameterization. Ideally we would like to guide mesh refinement using measures of model resolution and variance, since it is already known that there is a fundamental trade-off between these quantities in any linear inverse problem [*Backus and Gilbert* 1970; see also *Menke* 1989]. This is the philosophy behind the earlier static parameterizations built around ray path densities. Recent work suggests that it may be possible to calculate model resolution and covariance measures for large tomographic systems [*Nolet et al.* 1999; *Yao et al.* 1999]. At present these do not yet appear to have been used in applications of adaptive tomography.

One must be careful in interpreting a laterally varying velocity model which is itself built on a laterally varying parameterization. In classical tomography one would be suspicious of structures in velocity models which correlate with those in the underlying mesh. However, if the guiding principle in the design of an irregular parameterization is to mimic the resolving power of the data, then one would hope the Earth model would be well recovered in regions where the resolution was highest, and hence the mesh was finest. This process will tend to encourage a correlation between trends in the model and trends in the parameterization. In adaptive tomography then, the mesh becomes part of the solution, and we may have to change the way we interpret tomographic models.

5. CONCLUSIONS

In this article we have summarized recent attempts at using irregular parameterizations in tomographic problems. Even though the seismic community have only recently begun to consider this approach, its origins can be traced back more than twenty years (even in seismic applications). We have outlined solutions to the various geometrical problems involved in building complex irregular meshes in 3-D. The three examples illustrate the range of distance scales over which tomographic techniques find applications.

We have discussed the different ways in which irregular parameterizations have been used in seismic tomography, e.g. triangular or cubic based meshes, static or adaptive parameterizations, etc. At present it is not clear that any one approach is demonstratively better than any of the others. This is largely because there have been very few studies comparing results produced with regular and irregular meshes, or static versus adaptive tomography. These types of studies need to be done in order to find out whether the effort in implementing the more complicated procedures is justified by the improvement in the tomographic results. There is currently no clear guiding theory on how to adapt a 2-D or 3-D tomographic mesh in an optimal manner, although some techniques proposed for non-seismic tomographic problems, may well be useful in this regard. It would be interesting to see their application to seismic problems.

Ultimately in seismic tomography, one is always trying to image a laterally varying Earth using data sets with laterally varying resolving power. As seismic networks

continue to develop one would expect an improvement in distribution of seismic receivers across the globe; however, the uneven spread of sources will of course remain. It seems therefore that the Earth will continue to be sampled non-uniformly, and hence interest in irregularly parameterized tomography is set to continue.

Acknowledgments. We are grateful to Todd Nicholson and Eric Debayle for use of Plate 1 and Figure 6, and Alexei Gorbatov for his tomographic models used in Figure 1 and Plate 1. Figure 1 was produced with the *Tomoeye* software of *Gorbatov et al.* [2004]. Dimitri Komatitsch provided constructive comments on an earlier draft. Hend Ben Ameur and Trond Mannseth kindly provided preprints of their work. Computer software and related material can be found at `http://rses.anu.edu.au/seismology/projects/tireg`.

References

Abers, G. G., and S. W. Roecker, Deep structure of an arc-continent collision: Earthquake relocation and inversion for upper mantle P and S wave velocities beneath Papua New Guinea, *J. Geophys. Res.*, **96**, 6379-6401, 1991.

Backus, G. E., and J. F. Gilbert, Uniqueness in the inversion of inaccurate gross Earth data, *Philos. Trans. R. Soc. London.*, **266**, 123-192, 1970.

Barber, B., D. P. Dobkin, and H. Huhdanpaa, The Quickhull Algorithm for Convex Hull, The Geometry centre technical report GCG53, The Geometry Centre, Univ. of Minnesota, Minneapolis, 1993.

Ben Ameur, H., G. Chavent, and J. Jaffré, Refinement and coarsening indicators for adaptive parametrization: application to the estimation of hydraulic transmissivities, *Inverse problems*, **18**, 775-794, 2002.

Bentley, J. L., Multidimensional binary search trees used for associative searching, *Communications of the ACM*, **18**, 509-517.

Bijwaard, H., W. Spakman, and E. R. Engdahl, Closing the gap between regional and global travel time tomography, *J. Geophys. Res.*, **103**, 30055-30078, 1998.

Bijwaard, H. and W. Spakman, Non-linear global P-wave tomography by iterated linearized inversion, *Geophys. J. Int*, **141**, 71-82, 2000.

Böhm, G., P. Galuppo, and V. Vesnaver, 3D adaptive tomography using Delaunay triangles and Voronoi polygons, *Geophys. Prosp.*, **48**, 723-744, 2000.

Chiao, L. Y., and B. Y. Kuo, Multiscale seismic tomography, *Geophys. J. Int*, **145**, 517-527, 2001.

Chou, C. W., and J. R. Booker, A Backus-Gilbert approach to inversion of travel time data

for three-dimensional velocity structure, *Geophys. J. R. astr. Soc.*, **59**, 325-344, 1979.

Constable, C. G., R. L. Parker, and P. B. Stark, Geomagnetic field models incorporating frozen flux constraints, *Geophys. J. Int*, **113**, 419-433, 1993.

Curtis, A., and R. Snieder, Reconditioning inverse problems using the genetic algorithm and revised parameterization, *Geophysics*, **62**, 1524-1532, 1997.

Debayle, E. and M. Sambridge, Inversion of massive surface wave data sets: model construction and resolution assessment *J. Geophys. Res.*, *in press*, 2004.

Dziewonski, A. M., Global seismic tomography of the mantle, *Rev. Geophys.*, **33**, 419-423, 1995.

Eberhart-Phillips, D., Three-dimensional velocity structure in northern California coast ranges from inversion of local earthquake arrival times, *Bull Seismol. Soc. Am.*, **76** 1025-1052, 1986.

Engdahl, E. R., R. D. van der Hilst, and R. Buland, Global teleseismic earthquake relocation with improved travel times and procedures for depth determination. *Bull Seismol. Soc. Am.*, **88**, 722-743, 1998.

Faletič, R, *Seismic Tomography with a self-adaptive parameterisation*, *Honours thesis*, Australian National University, 1997.

Fukao, Y., M. Obayashi, H. Inoue, and M. Nenbai, Subducting slabs stagnant in the mantle transition zone, *J. Geophys. Res.*, **97**, 4809-4822, 1992.

Gorbatov, A., Y. Fukao, S. Widiyantoro, Application of a three-dimensional ray tracing technique to global P, PP and Pdiff traveltime tomography, *Geophys. J. Int*, **146**, 583-595, 2001.

Gorbatov, A., A. Limaye, and M. Sambridge, Tomoeye: a Matlab package for analysis of 3-D

tomographic models, *Geochem. Geophys. Geosyst.*, *submitted*, 2004.

Grand, S. P., R. D. van der Hilst, and S. Widiyantoro, Global seismic tomography: a snapshot of convection in the Earth, *GSA today*, **7**, 1-7, 1997.

Grimstad, A-A., T. Mannseth, G. Nævdal and H. Urkedal, Adaptive multiscale permeability estimation *Computational Geosciences*, **7**, 1-25, 2003.

Gudmundsson, O. and M. Sambridge, A regionalized upper mantle (RUM) seismic model, *J. Geophys. Res.*, **103**, No. B4, 7121-7136, 1998.

Iyer, H. M. and K. Hirahara, (Eds.), Seismic Tomography - Theory and Practice, Chapman & Hall, London, 9-22, 1993.

Kennett, B. L. N., E. R. Engdahl, and R. Buland, Constraints on seismic velocities in the Earth from travel times, *Geophys. J. Int*, **122**, 109-124, 1995.

Lutter, W. J. and R. L. Nowack, Inversion for crustal structure using reflections from the PASSCAL Ouachita experiment, *J. Geophys. Res.*, **95** 4633-4646, 1990.

Masters, T. G., and P. M. Shearer, Seismic Models of the Earth: Elastic and Anelastic, in edited by T. J. Ahrens, pp 88-103, Amer. Geophys. Union., Washington, 1995.

Menke, W., *Geophysical data analysis: discrete inverse theory*, (Rev. ed), Academic Press, San Diego, 1989.

Michelini, A., An adaptive-grid formalism for travel time tomography, *Geophys. J. Int*, **121**, 489-510, 1995.

Montelli R., Nolet G., Dahlen F.A., Masters G., Hung S-H, Global time tomography of finite frequency waves with optimized tetrahedral grids, *Eos. Trans. AGU*, **82**(47), Fall Meet. Suppl., Abstract S32B-0636, 2001.

Neele, F., J. VanDecar, and R. Snieder, The use of P wave amplitude data in a joint

inversion with travel times for upper mantle velocity structure, *J. Geophys. Res.*, **98** 12,033-12054, 1993.

Nolet, G., S. P. Grand, and B. L. N. Kennett, Seismic heterogeneity in the upper mantle, *J. Geophys. Res.*, **99**, 23753-23766, 1994.

Nolet G., R. Montelli, and J. Virieux, Explicit, approximate expressions for the resolution and a posteriori covariance of massive tomographic systems *Geophys. J. Int*, **138**, 36-44, 1999.

Okabe, A., B. Boots, and K. Sugihara, *Spatial Tessellations: Concepts and Applications of Voronoi Diagrams*, John Wiley & Sons, Chichester, England, 1992.

Press, W. H., B. P. Flannery, A. T. Saul, and W. T. Vetterling, *Numerical Recipes* (2nd ed.), Camb. Univ. Press., Cambridge, 1992.

Rawlinson, N. and M. Sambridge, Irregular interface parameterization in 3-D wide-angle seismic traveltime tomography *Geophys. J. Int*, **155**, 79-92, 2003.

Rawlinson, N., G. A. Houseman, and C. D. N. Collins, Inversion of seismic refraction and wide-angle reflection traveltimes for 3-D layered crustal structure, *Geophys. J. Int*, **145**, 381-401, 2001a.

Rawlinson, N., G. A. Houseman, C. D. N. Collins, New evidence of Tasmania's tectonic history from a novel seismic experiment *Geophys. Res. Lett.,* **28**, 3337-3340, 2001b.

Ritzwoller, M. H., and E. M. Lavely, Three-dimensional seismic models of the Earth's mantle, *Rev. Geophys.*, **33**, 1-66, 1995.

Romanowicz, B., Seismic tomography of the Earth's mantle, *Ann. Rev. earth Planet. Sci.* **19**, 77-99, 1991.

Sambridge, M., Non-linear arrival time inversion: constraining velocity anomalies by seeking

smooth models in 3-D, *Geophys. J. Int*, **102**, 653-677, 1990.

Sambridge, M., J. Braun, and H. McQueen, Geophysical parametrization and interpolation of irregular data using natural neighbours, *Geophys. J. Int*, **122**, 837-857, 1995.

Sambridge, M. and O. Gudmundsson, Tomographic systems of equations with irregular cells, *J. Geophys. Res.*, **103**, No. B1, 773-781, 1998.

Sambridge, M. and R. Faletič, Adaptive whole Earth Tomography, *Geochem. Geophys. Geosyst.*, **4**, No. 3, doi:10.1029/2001GC000213, 5 March 2003.

Samet, H., Spatial data structures, in *Modern database systems: The Object Model, Interoperability and Beyond*, W. Kim (Ed.), Addison Wesley/ACM Press, Reading, MA, 361-385, 1995.

Shearer, P. M., *Introduction to seismology*, Camb. Univ. Press., Cambridge, U.K., 1999.

Spakman, W. and H. Bijwaard, Optimization of cell parameterizations for tomographic inverse problems, *Pure appl. Geophys.*, **158**, 1401-1423, 2001.

Su, W. J. and A. M. Dziewonski, Simultaneous inversion for 3-D variations in shear and bulk velocity in the mantle, *Phys. Earth Planet. Inter.,* **100**, 135-156, 1997.

Su, W. J., R. L. Woodward and A. M. Dziewonski, Degree 12 model of shear velocity heterogeneity in the mantle, *J. Geophys. Res.*, **99**, 6945-6980, 1994.

Tarantola, A. and A. Nercessian, Three-dimensional inversion without blocks, *Geophys. J. R. astr. Soc.*, **76**, 299-306, 1984.

Thomson, C. J., D. Gubbins, Three-dimensional lithospheric modelling at NORSAR: linearity of the method and amplitude variations from anomalies, *Geophys. J. R. astr. Soc.*, **71**, 1-36, 1982.

Thurber, C. H., Earthquake locations and three-dimensional crustal structure in the Coyote

Lake area, central California, *J. Geophys. Res.*, **88**, 8226-8236, 1983.

VanDecar, J. C., D. E. James, M. Assumpção, Seismic evidence for a fossil mantle plume beneath South America and implications for plate driving forces, *Nature*, **378**, 25-31, 1995.

van der Hilst, R. D., Widiyantoro, S. and E. R. Engdahl, Evidence for deep mantle circulation from global tomography, *Nature*, **386**, 578–584, 1997.

Vesnaver, A. L., Irregular grids in seismic tomography and minimum time ray tracing, *Geophys. J. Int*, **126**, 147-165, 1996.

Vesnaver, A., G. Böhm, G. Madrussani, and H. Granser, Depth imaging and velocity calibration by 3D adaptive tomography, *First Break*, **18**, 303-312, 2000.

Voronoi, M. G., Nouvelles applications des paramètres continus à la théorie des formes quadratiques, *J. reine Angew. Math.*, **134**, 198-287, 1908.

Wang, Z, and F. A. Dahlen, Spherical-spline parameterization of three dimensional earth models, *Geophys. Res. Lett.,* **22**, 3099-3102, 1995.

Wang, Z, J. Tromp, and G. Ekstrom, Global and regional surface-wave inversions: A spherical-spline parameterization, *Geophys. Res. Lett.,* **25**, 207-210, 1998.

Widiyantoro, S. and R. D. van der Hilst, Mantle structure beneath Indonesia inferred from high-resolution tomographic imaging, *Geophys. J. Int*, **130**, 167-182, 1997.

Williamson, P. R., Tomographic inversion in reflection seismology, *Geophys. J. Int*, **100**, 255-274, 1990.

Yao, Z. S., R. G. Roberts, and A.Tryggvason, Calculating resolution and covariance matrices for seismic tomography with the LSQR method, *Geophys. J. Int*, **138**, 886–894, 1999.

Zelt, C. A. and R. B. Smith, Seismic traveltime inversion for 2-D crustal velocity structure,

Geophys. J. Int, **108**, 16-34, 1992.

Zhou, H-W., A high resolution P-wave model for the top 1200 km of the mantle, *J. Geophys. Res.*, **101** 27,791-27,810, 1996.

M. Sambridge and N. Rawlinson, Centre for Advanced Data Inference, Research School of Earth Sciences, Institute of Advanced Studies, Australian National University, Canberra, A.C.T. 0200, Australia. (E-mail: malcolm@rses.anu.edu.au; nick@rses.anu.edu.au)

Received _____

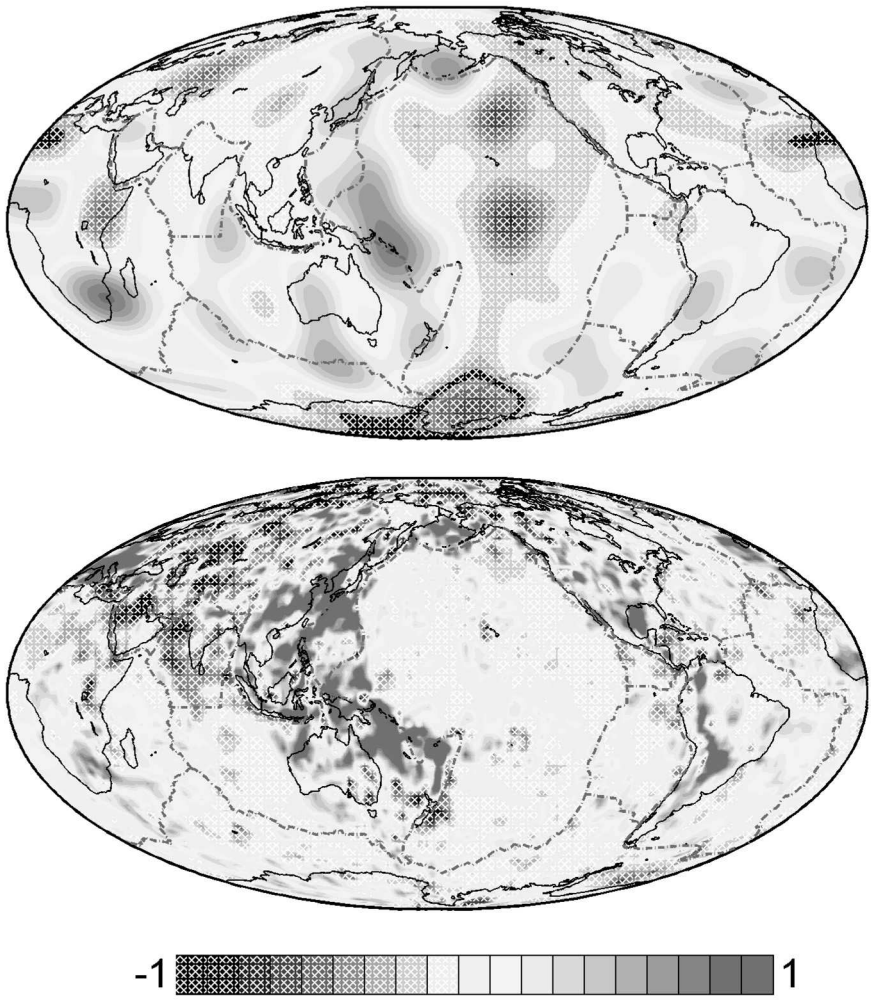

Figure 1. Two models showing different spatial scale lengths of parameterizations used in global body wave tomography. On the left the spherical harmonic model $SP12/WM13$ of *Su et al.* [1994] and on the right the high resolution block model of *Gorbatov et al.* [2001]

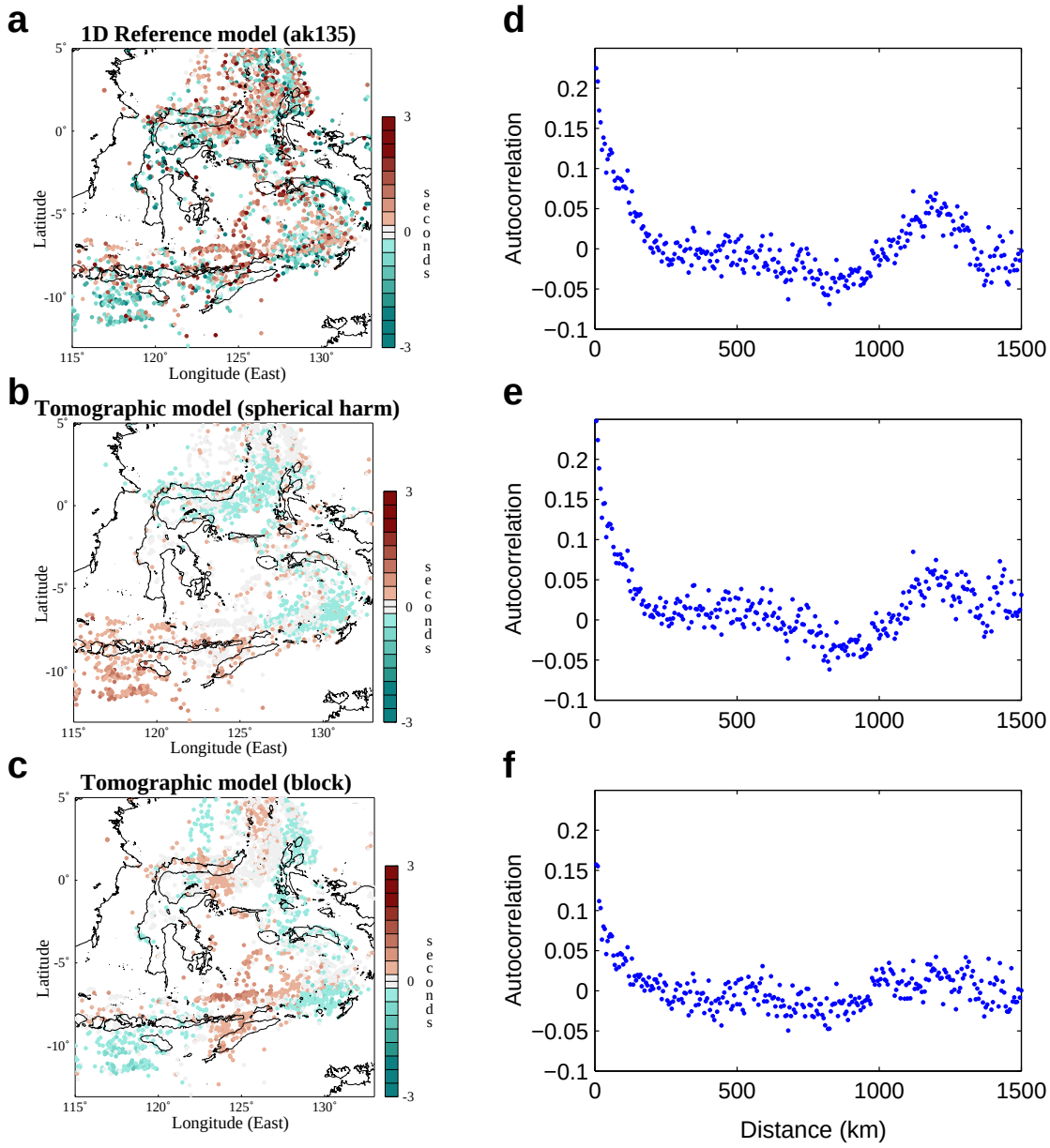

Plate 1. a) Arrival time residuals ($T_{obs} - T_{ak135}$), of 1-D reference model $ak135$ plotted for station MAT in Japan, shown as a function of source position, for events in the Indonesian region; b) similar to a) but for the long wavelength spherical harmonic model MK12/WM13, ($T_{SH} - T_{ak135}$); c) similar to a) but for the high resolution block model of *Gorbatov et al.* [2001], ($T_{block} - T_{ak135}$). d) The auto-correlation function of the residuals in a) (see text for definition); e) the auto-correlation function for the spherical harmonic residuals ($T_{SH} - T_{obs}$); f) the auto-correlation function for the block residuals ($T_{block} - T_{obs}$).

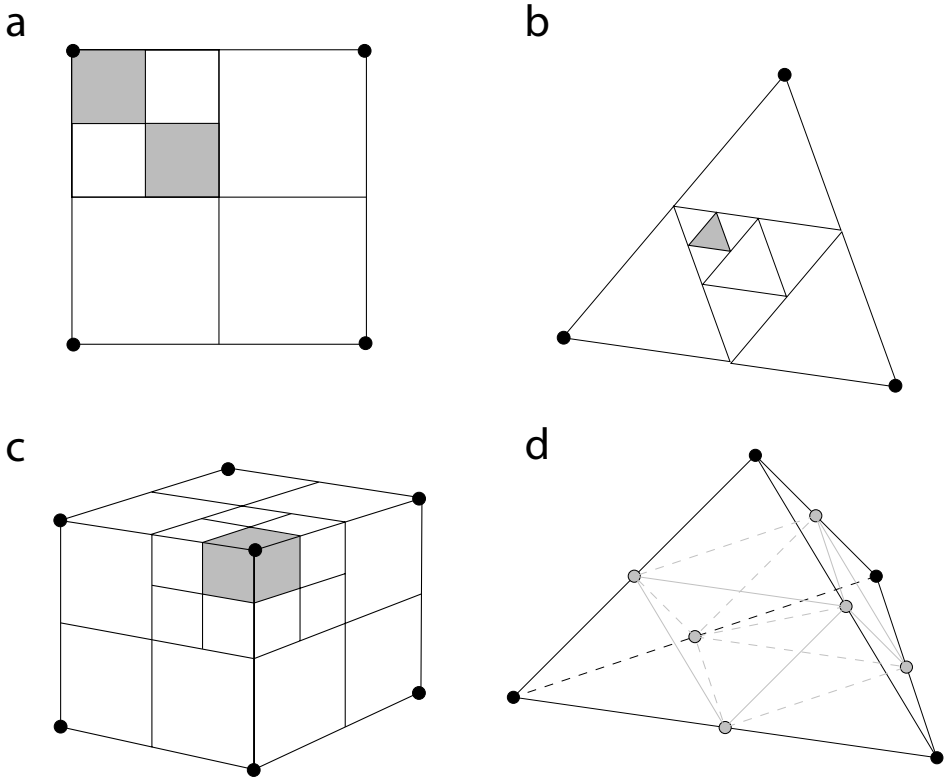

Figure 2. Examples of ways in which tomographic cells can be sub-divided in a multi-scale parameterization. At each division a) squares and b) triangles are divided into four self-similar shapes, whereas c) cubes and d) tetrahedra produce eight sub-divisions. In the latter case not all smaller tetrahedra have the same shape.

A

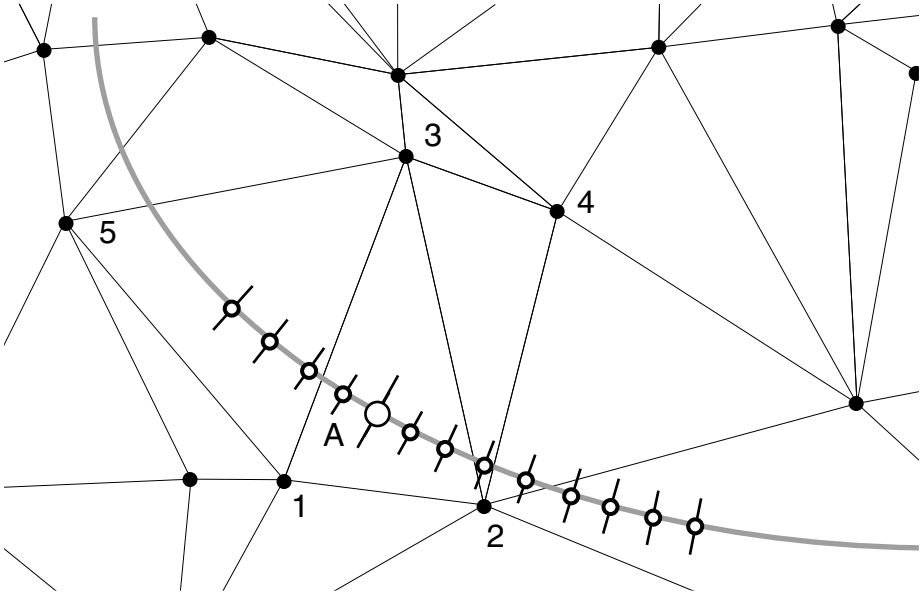

B

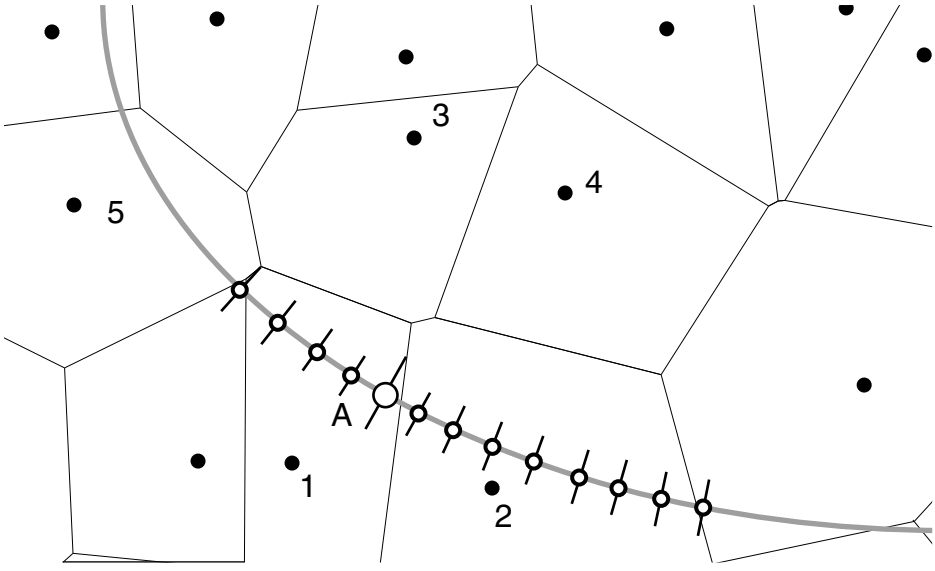

Figure 3. Calculating Fréchet derivatives of travel times with respect to model parameters by integration of basis functions along a reference ray a) in Delaunay triangles, b) in Voronoi (nearest neighbour) cells. In the numerical integration the cell containing each point along the ray must be found.

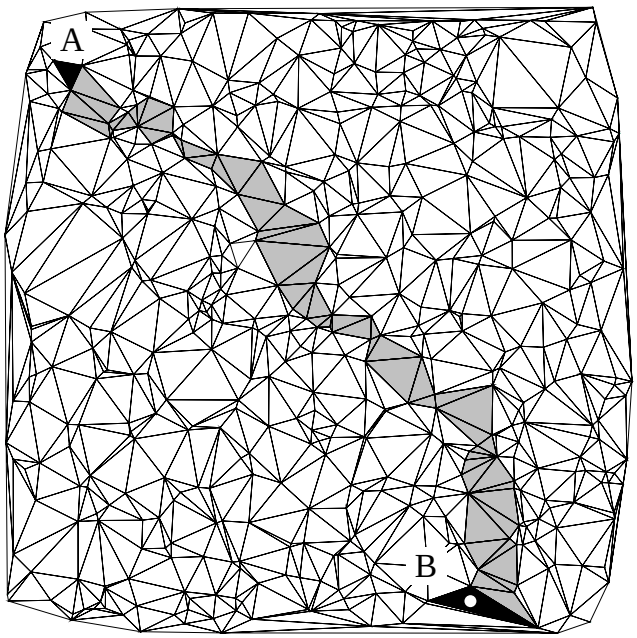

Figure 4. An example of the cell location algorithm described in section 3.2 in a triangular parameterization. Starting from a first guess cell A, the algorithm only tests the shaded cells in its 'walk' to the correct triangle B, containing the point to be located (white circle). The same style of procedure can be applied to meshes built from other convex shapes.

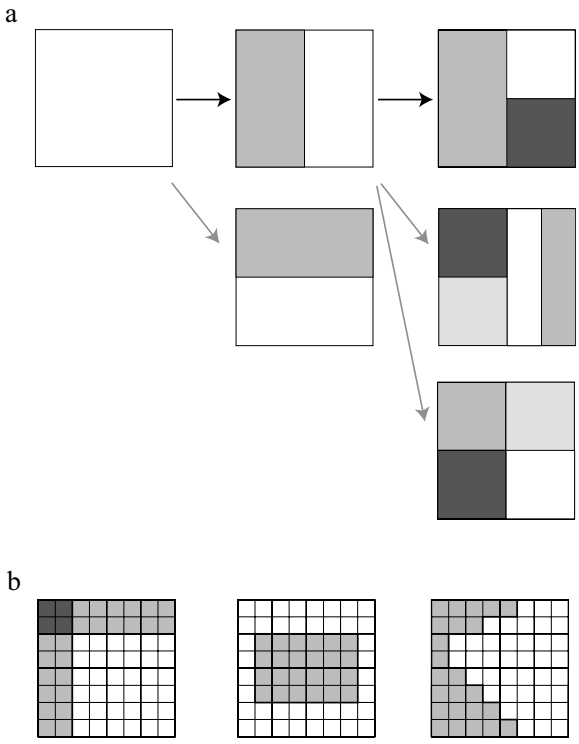

Figure 5. a) An example of the multi-scale adaptive tomography technique of *Grimstad et al.* [2002]. At each iteration the current model is sub-divided and only the parameterization which has the best predicted data fit improvement is selected (see text). The black arrow points to the chosen model. b) Three examples of the way a parameterization might be sub-divided in the adaptive discretization technique of *Ben Ameur et al.* [2002]. The thick line represents the 'cut path' through an existing parameterization producing multiple new regions (shaded). This Figure also serves as an example of a 'bottom up' style parameterization built by joining together regular square cells.

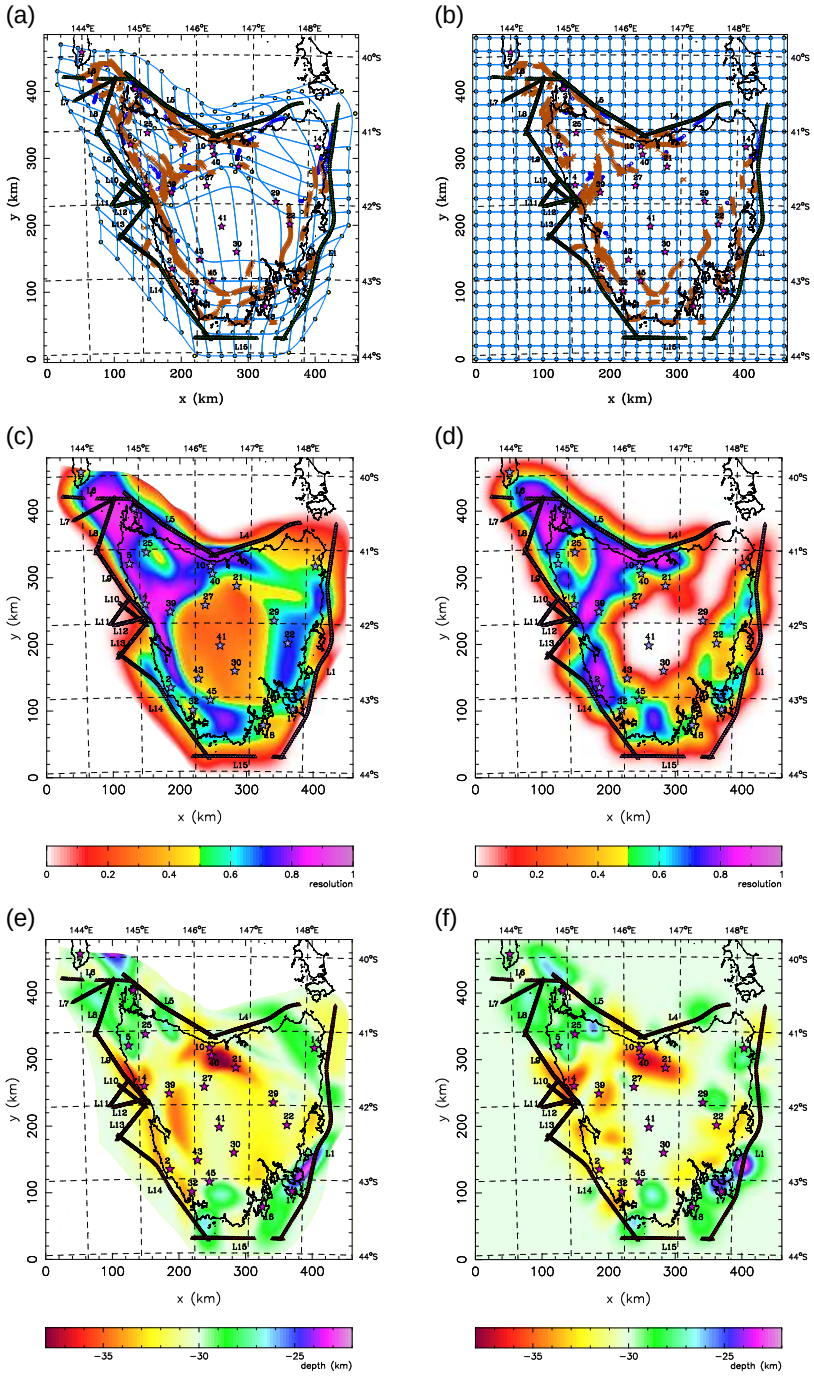

Plate 2. Comparison of inversion results using regular and irregular grids and wide-angle data from Tasmania. In all diagrams, stars indicate receiver positions and small triangles indicate shot points; contiguous triangles form shot lines. (a) Ray interface hit points and surface patches for the irregular grid. Refracted ray hits are denoted by blue crosses and reflected ray hits are denoted by brown crosses. Interface nodes are represented by dots and thin blue lines represent surface patch boundaries; (b) same as (a) but for the regular grid. (c) Diagonal elements of the resolution matrix for the irregular grid solution; (d) same as (c) but for the regular grid. (e) Solution model for the irregular

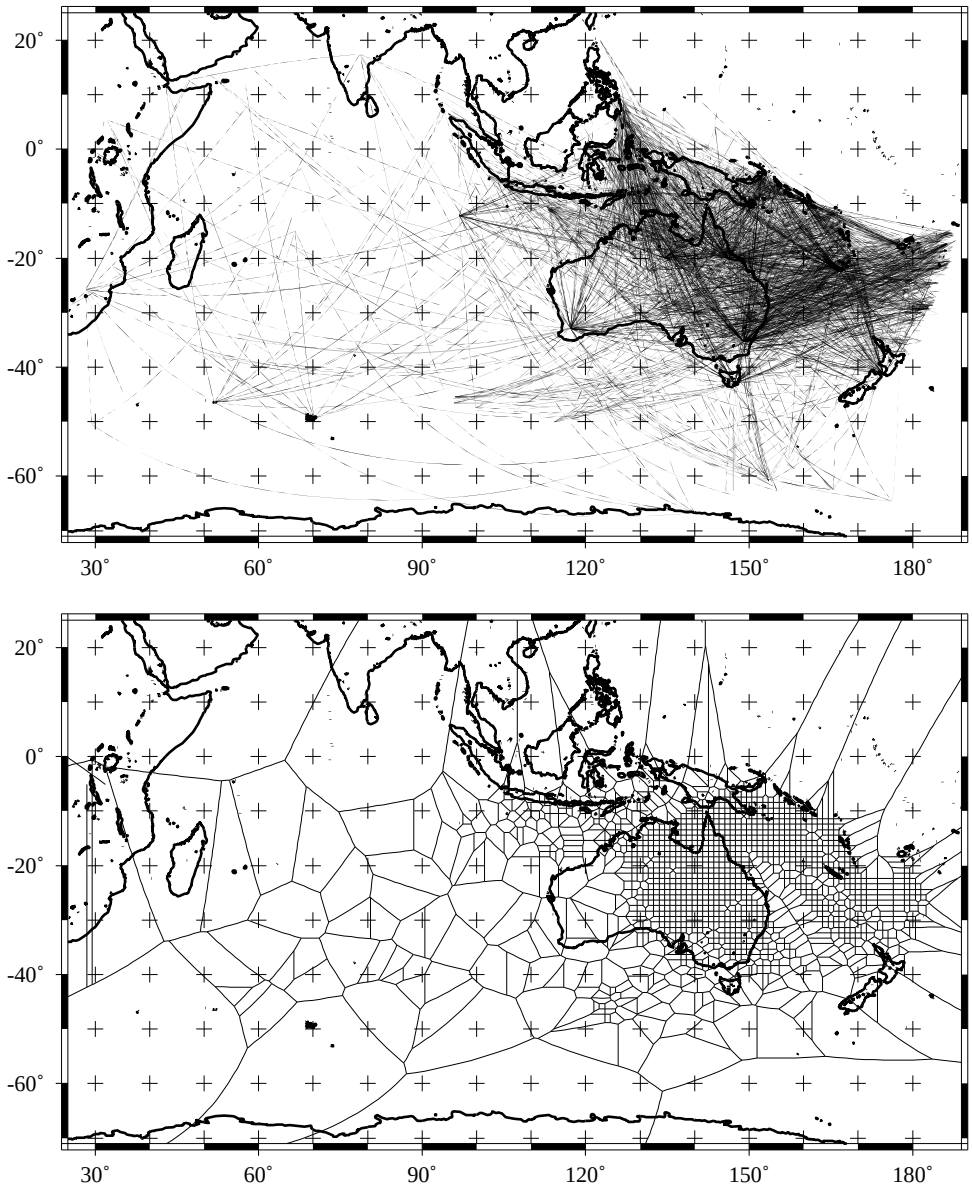

Figure 6. a) Ray paths of surface waves from permanent stations in the Indian ocean and portable broadband arrays on the Australian continent. Note the large variation in ray path densities. b) Spherical Voronoi (nearest neighbour) cells derived from the ray paths in a) to represent regions where azimuthal anisotropy and lateral heterogeneity are resolvable.

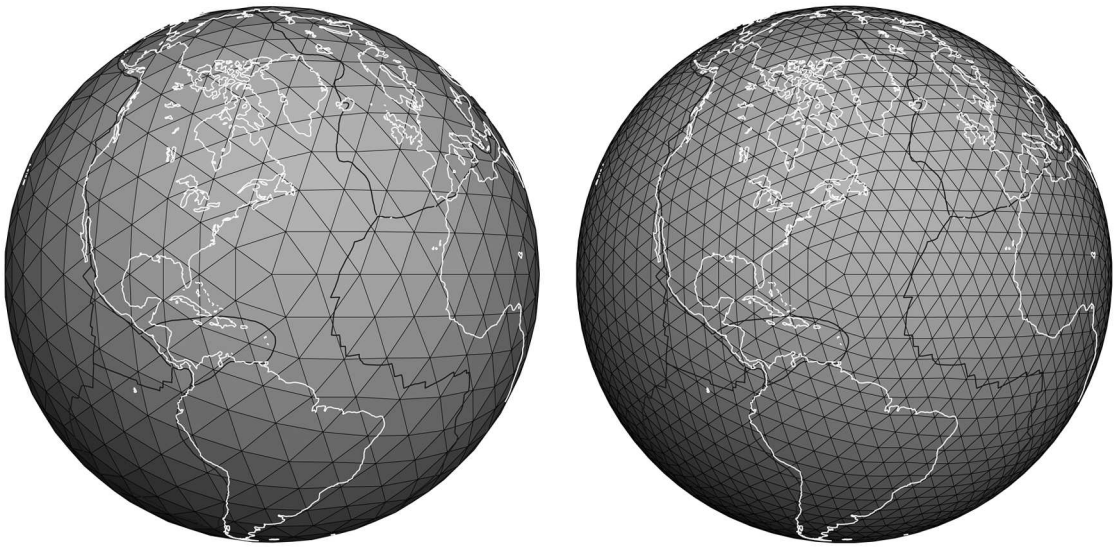

Figure 7. Two uniform subdivisions of a sphere into spherical triangles using the approach of *Wang and Dahlen* [1995]. These are used as the starting point of the adaptive whole Earth tomography examples shown in section 4. Note that there is virtually no distortion in the shape of the triangular cells at the poles.

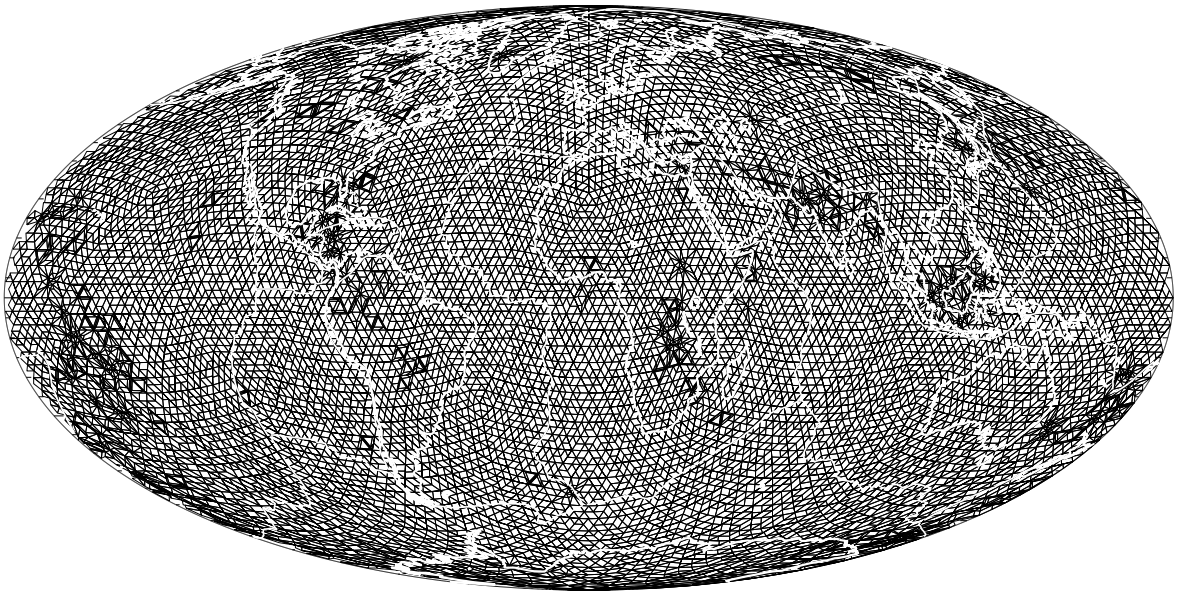

Figure 8. A slice, at 1300 km depth, through the first of four 3-D tetrahedral meshes produced during the whole Earth adaptive tomography study of *Sambridge and Faletič* [2003]. The mesh was refined automatically in areas where the largest lateral velocity gradients were found, and these correspond to well known features in the mantle (e.g. subducted Tethys ocean and Farallon plate as well as the great African plume). A further refinement of the parameterization is shown for the Australian region in Figure 9.

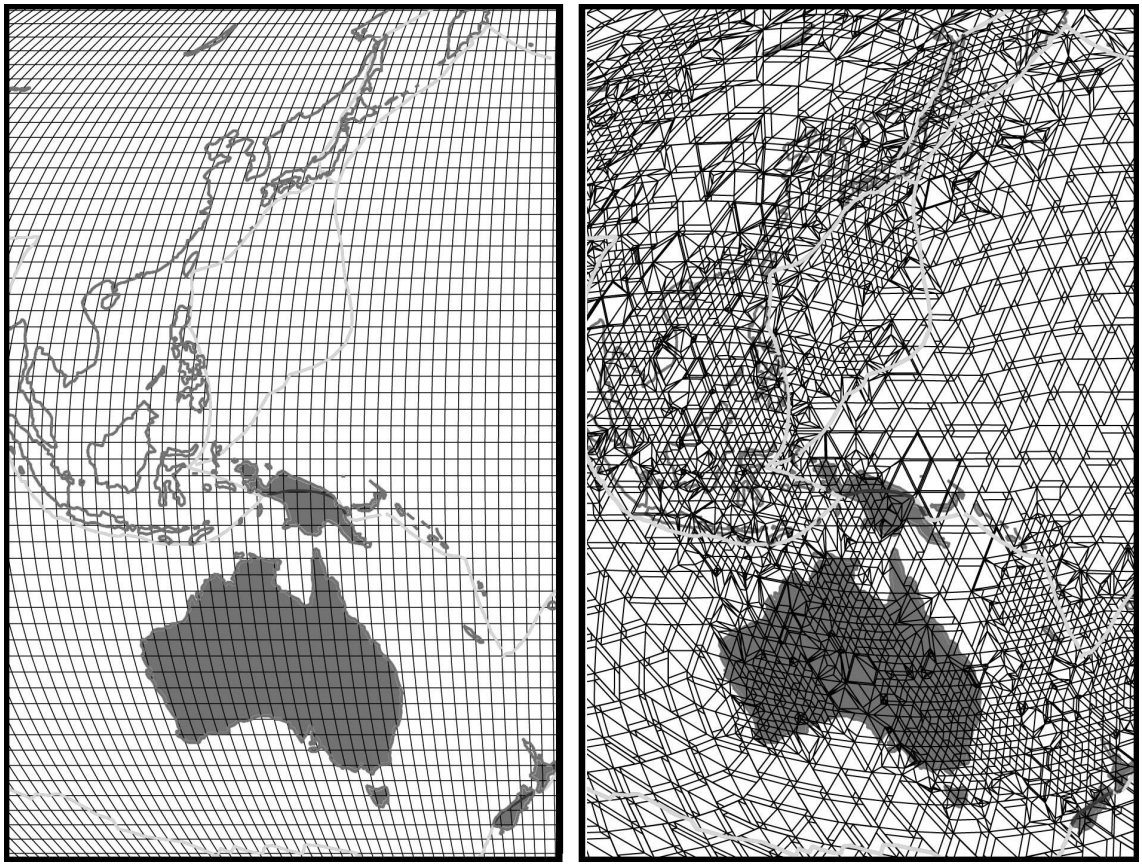

Figure 9. A slice at 500 km depth through the final parameterization of *Sambridge and Faletič* [2003] for the Australian region (right panel) together with a uniform 2° × 2° mesh for comparison. Note how the tetrahedral mesh has been refined in regions where subduction dominates. This type of parameterization can become very complex, especially in 3-D.